JOURNAL OF PROPULSION AND POWER
Vol. 17, No. 4, July–August 2001

Random Packs and Their Use in Modeling Heterogeneous Solid Propellant Combustion

S. Kochevets,* J. Buckmaster,† T. L. Jackson,‡ and A. Hegab§
University of Illinois at Urbana–Champaign, Urbana, Illinois 61801

It is shown that random packs of spheres of various sizes can be constructed that model ammonium–perchlorate-in-binder propellants in the sense that both the size distributions and the packing fractions of industrial propellant packs can be matched. Strategies for dealing with fractional numbers of large particles are addressed, as are strategies for dealing with a large number of very fine particles (fine powder). Fine powder is necessary in a three-dimensional pack to achieve the required stoichiometric ratio of ammonium perchlorate to fuel binder, but is not necessary in a two-dimensional (disk) pack. Some preliminary calculations of the two-dimensional combustion field supported by a disk pack are presented, in which full coupling between the gas phase, the condensed phase, and the retreating nonplanar propellant surface is accounted for.

Nomenclature

$D_{1,2}$	=	reaction rate constants
d_j	=	mean diameter of particles
$E_{1,2}$	=	activation energies
L	=	length of a pack edge
N	=	total number of particles
N_j	=	number of particles in the jth class
n_j	=	number fraction of particles in the jth diameter classs
$n_{1,2}$	=	pressure exponents
R_u	=	universal gas constant
$R_{1,2}$	=	reaction rates
r_b	=	surface regression rate
T	=	temperature
V_j	=	volume of particles in the jth class
v_j	=	volume fraction of particles in the jth class
X	=	mass fraction of ammonium perchlorate (AP)
Y	=	mass fraction of fuel binder
Z	=	mass fraction of AP decomposition products
η	=	surface function
ϕ	=	surface location
ψ	=	level set function defining the pack

Subscripts

AP	=	AP
B	=	binder
c	=	condensate

I. Introduction

IT has long been recognized that the burning rate of a heterogeneous propellant is influenced by the propellant morphology, by the size and size distribution of the ammonium perchlorate (AP) particles. It follows that any serious attempt to simulate propellant burning numerically must incorporate a packing algorithm, a strategy for defining and constructing a model propellant. Lattice (or crystal) packs are easily defined,[1] but do not reflect the random nature of a true propellant. For this, a random packing algorithm must be used, and a suitable one is identified and discussed in Ref. 2. This algorithm is dynamic in nature and can closely pack spheres of arbitrary size.

The calculations of Ref. 2 are restricted to bimodal packs, two sphere sizes, and no serious attempt is made to simulate true propellants. A good portion of the present paper is concerned with an examination of experimental AP size data, and the use of these data to define realistic packs with packing fractions (volume percentage of AP) that closely approximate those of true propellants.

The remainder of the paper describes preliminary flame calculations for which the propellant data are defined by a random pack. These calculations incorporate in as simple fashion as possible the following ingredients: AP decomposition; reaction between the products of the AP decomposition and the binder gases; unsteady heat conduction within the solid, allowing for the different mechanical and thermal properties of the AP and binder; an unsteady nonplanar regressing surface; temperature-dependent transport in the gas phase; and an Oseen approximation in the gas phase, which bypasses the momentum equation. Our code can incorporate the momentum equation when desired, but we have not chosen to do so in the preliminary results, which we present here. Further discussion of this issue, together with flame calculations for a sandwich propellant in which a full accounting of the Navier–Stokes equations is incorporated, may be found in Ref. 3.

II. Packing a Propellant

The industry constructs propellants by mixing a selection of AP cuts in suitable proportions. Each cut is characterized by a nominal size, 200, 50, 20 μm, etc., but there is a wide range of sizes within each cut. It is instructive to examine some true cuts, and here we show data provided by Thiokol Corporation, courtesy of R. Bennett.

The first three columns of Table 1 define experimental histogram data for a 200 μm cut. These data are acquired by passing the AP through a sequence of sieves of ever-decreasing mesh diameter (first column). The second column shows the percentage (by volume) of AP that passes through each sieve. Thus, 100% passes through the 592.0-μm sieve, that is, there are no particles larger than 592.0 μm, but only 99.96% passes through the 542.9-μm sieve, so that 0.04% by volume (third column) of the particles have diameter between 542.9 and 592.0 μm. At the other end of Table 1, we see that there are no particles smaller than 52.33 μm, and 0.15% by volume have diameters between 52.33 and 57.06 μm. It is convenient to replace each diameter interval by its mean so that, for example, 0.04% of the AP has diameter 567.45 μm (fourth column), the mean of 592.0 and 542.9.

The volume fractions can be converted to number fractions in the following fashion. Given a portion of AP, suppose that N_j of the

Received 17 November 2000; revision received 18 March 2001; accepted for publication 20 March 2001.

*Graduate Student, Department of Mechanical and Industrial Engineering, 1206 W. Green Street; kochevet@uiuc.edu.

†Professor, Department of Aeronautical and Astronautical Engineering, 104 S. Wright Street; limey@uiuc.edu. Associate Fellow AIAA.

‡Senior Research Scientist, Center for the Simulation of Advanced Rockets, 1304 W. Springfield Avenue; tlj@csar.uiuc.edu.

§Postdoctoral Associate, Department of Aeronautical and Astronautical Engineering, 104 S. Wright Street; hegab@uiuc.edu.

Table 1 Experimental 200-μm AP data; $\{N_j\}$ are calculated for 3000 particle pack

Channel, μm	% Pass	% In channel	Mean diameter d_j	No. fraction n_j	N_j
592.0[a]	100	0.04	567.45	0.000011	0.034
542.9[a]	99.96	0.18	520.35	0.000066	0.198
497.8[a]	99.78	0.52	477.15	0.000247	0.742
456.5[a]	99.26	1.27	437.55	0.000784	2.351
418.6	97.99	2.64	401.25	0.00211	6.337
383.9	95.35	4.33	367.95	0.00449	13.479
352.0	91.02	6.50	337.4	0.00875	26.242
322.8	84.52	8.26	309.4	0.01442	43.245
296.0	76.26	9.59	283.7	0.02171	65.127
271.4	66.67	10.15	260.65	0.02963	88.882
249.9	56.52	9.87	239.05	0.03735	112.040
228.2	46.65	9.19	218.75	0.04538	136.142
209.3	37.46	8.13	200.6	0.05206	156.178
191.9	29.33	6.93	183.95	0.05755	172.645
176.0	22.40	5.61	168.7	0.06040	181.192
161.4	16.79	4.41	154.7	0.06157	184.709
148.0	12.38	3.31	141.85	0.05994	179.830
135.7	9.07	2.44	130.1	0.05727	171.822
124.5	6.63	1.79	119.3	0.05449	163.476
114.1	4.84	1.31	109.4	0.05172	155.146
104.7	3.53	0.95	100.33	0.04862	145.865
95.96	2.58	0.71	91.98	0.04716	141.481
88.00	1.87	0.53	84.35	0.04565	136.944
80.70	1.34	0.41	77.35	0.04579	137.380
74.00	0.93	0.31	70.93	0.04490	134.708
67.86	0.62	0.25	65.045	0.04696	140.870
62.23	0.37	0.22	59.645	0.05359	160.776
57.06	0.15	0.15	54.695	0.04739	142.157
52.33	0.00	0.00	——	——	——

[a]Diameter classes that are consolidated.

particles have diameter d_j, $j = 1, M$. The volume of these particles is

$$V_j = (\pi/6) d_j^3 N_j \tag{1}$$

and the total volume is

$$V = \frac{\pi}{6} \sum_{i=1}^{M} d_i^3 N_i \tag{2}$$

Then the volume fraction of the class j is

$$v_j = \frac{d_j^3 N_j}{\sum_{i=1}^{M} d_i^3 N_i} \tag{3a}$$

that is,

$$v_j \sum_{i=1}^{M} {d_i}^3 N_i = {d_j}^3 N_j, \qquad j = 1, M \tag{3b}$$

With the volume fractions defined by the third column, Eqs. (3b) define a linear homogeneous system, which can be solved for the number fractions

$$n_j = \frac{N_j}{\sum_{i=1}^{M} N_i} \tag{4}$$

shown in the fifth column.

There are a number of ways in which these data can be used to define a pack, and we shall now describe one such procedure. First, the number of particles in the pack is assigned. At the present time, because of limitations inherent in the code, this number is best kept below 10,000 when running on a one-processormachine. Then each n_j can be converted to an N_j, and in this way a table with the values of d_j and N_j is defined.

It is typically the case that the first entries N_1, N_2, etc., are significantly less than 1, and so it is necessary to consolidate the large diameter data. There is a certain arbitrariness in how this consolidation is done, but for the 200-μm data, the first four classes with diameters 567.45, 520.35, 477.15, and 437.55 μm have been consolidated into a single class of diameter 454.25 μm, the volume-weighted average. There are 3.325 particles in this class, the sum of N_1, N_2, N_3, and N_4, defined for 3000 particles. Additional consolidations are necessary, in general, but not for this example.

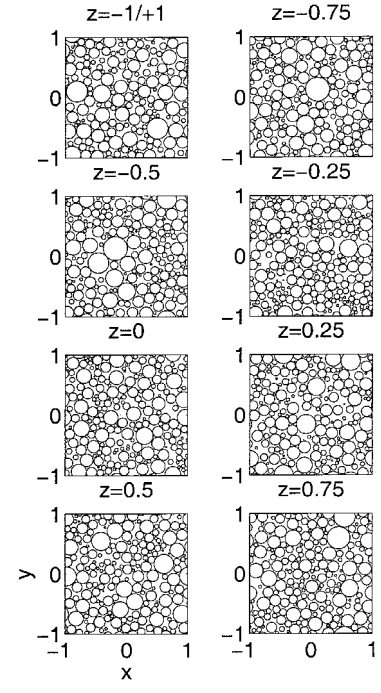

Fig. 1 Slices through a 200-μm cut, packing density 0.6559; slices at $z = +1$ and -1 are equal.

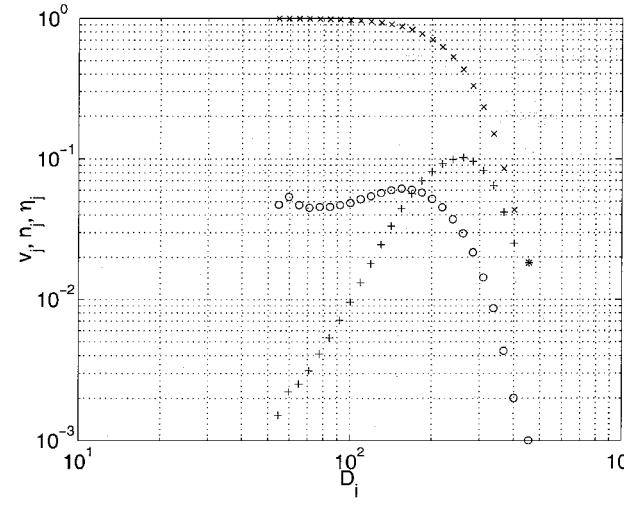

Fig. 2 Volume fraction (+), number fraction (○), and partial volume fraction (×) as a function of particle diameter for the 200-μm data.

When the N_j are rounded off to integer values, the set $\{d_j, N_j\}$ defines data for a pack. (Roundoff reduces the number of particles to 2998.) Slices through such a pack within a cube of side 2 are shown in Fig. 1, and the packing fraction is 0.6559, a value not much greater than the 0.625 achieved for a monomodal pack.[2] The pack is calculated in a nondimensional context, and to attach a physical value to the length L of a cube edge we can use the formula

$$\frac{\pi}{6} \sum_{i=1}^{N} N_i d_i^3 = (0.6559) L^3 \tag{5}$$

The packing fraction achieved here for the 200-μm data is significantly less than the value required for a stoichiometric AP/binder mix ($\sim$0.78), a reflection of the cleanness of the cut, the limited volume of small particles. Figure 2 shows volume fraction, number fraction (after consolidation), and the partial volume fraction

$$\eta_j = \sum_{i=1}^{j} v_i, \qquad (\eta_N = 1) \tag{6}$$

as a function of particle diameter.

Table 2 Experimental 20-μm AP data

Channel, μm	% Pass	% In channel	Mean diameter d_j	No. fraction n_j
176.0	100	0.18	168.7	0.000000024
161.4	99.82	0.26	154.7	0.000000044
148.0	99.56	0.25	141.85	0.000000055
135.7	99.31	0.27	130.1	0.000000077
124.5	99.04	0.30	119.3	0.000000111
114.1	98.74	0.35	109.4	0.000000169
104.7	98.39	0.41	100.33	0.000000256
95.96	97.98	0.48	91.98	0.000000389
88.00	97.50	0.59	84.35	0.000000620
80.70	96.91	0.71	77.35	0.000000968
74.00	96.20	0.87	70.93	0.000001538
67.86	95.33	1.06	65.045	0.000002430
62.23	94.27	1.27	59.645	0.000003776
57.06	93.00	1.49	54.695	0.000005745
52.33	91.51	1.73	50.155	0.000008651
47.98	89.78	1.97	45.990	0.000012777
44.00	87.81	2.19	42.175	0.000018418
40.35	85.62	2.39	38.675	0.000026065
37.00	83.23	2.57	35.465	0.000036
33.93	80.66	2.73	32.52	0.000050
31.11	77.93	2.84	29.82	0.000068
28.53	75.09	2.93	27.345	0.000090
26.16	72.16	2.99	25.075	0.000120
23.99	69.17	3.04	22.995	0.000158
22.00	66.13	3.06	21.085	0.000206
20.17	63.07	3.08	19.335	0.000269
18.50	59.99	3.08	17.73	0.000349
16.96	56.91	3.06	16.26	0.000449
15.56	53.85	3.00	14.915	0.000570
14.27	50.85	2.87	13.675	0.000708
13.08	47.98	2.85	12.54	0.000912
12.00	45.13	2.67	11.5	0.00111
11.00	42.46	2.55	10.545	0.00137
10.09	39.91	2.43	9.67	0.00170
9.250	37.48	2.34	8.866	0.00212
8.482	35.14	2.27	8.13	0.00267
7.778	32.87	2.24	7.455	0.00341
7.133	30.63	2.22	6.837	0.00438
6.541	28.41	2.23	6.27	0.00571
5.998	26.18	2.24	5.749	0.00744
5.500	23.94	2.26	5.272	0.00973
5.044	21.68	2.27	4.835	0.01267
4.625	19.41	2.26	4.433	0.01637
4.241	17.15	2.25	4.065	0.02113
3.889	14.90	2.22	3.728	0.02704
3.566	12.68	2.13	3.418	0.03365
3.270	10.55	1.98	3.135	0.04056
2.999	8.57	1.77	2.875	0.04702
2.750	6.80	1.50	2.636	0.05167
2.522	5.30	1.23	2.417	0.05496
2.312	4.07	0.95	2.216	0.05504
2.121	3.12	0.73	2.033	0.05481
1.945	2.39	0.55	1.864	0.05358
1.783	1.84	0.43	1.709	0.05435
1.635	1.41	0.34	1.567	0.05575
1.499	1.07	0.28	1.437	0.05953
1.375	0.79	0.24	1.318	0.06613
1.261	0.55	0.21	1.208	0.07506
1.156	0.34	0.20	1.108	0.09276
1.060	0.14	0.14	1.016	0.08422
0.972	0.00	0.00	——	——

When we apply the strategy described to the 20-μm cut in Table 2, a new difficulty emerges. The cut is dirty and contains a large number of small particles so that when N is assigned a reasonable value, a number of large bands of large-diameter classes have to be consolidated to ensure that there is at least one particle in each consolidation. When consolidation is necessary over a large range of diameters, the result is not reasonably representative of the true cut. One solution is to modify the cut by discarding all particles smaller than some specified cutoff diameter.

Thus, consider the 20-μm data and discard all particles smaller than 2 μm, totaling a volume fraction of 0.0239. The packing fraction for this modified cut will be smaller than the packing fraction for the true cut. With the choice $N = 3000$, the following classes are consolidated:

Table 3 Packing data 20-μm AP

d_j	N_j
43.553	1.103
28.457	1.033
23.937	1.814
21.085	1.347
19.335	1.759
17.730	2.281
16.260	2.938
14.915	3.731
13.675	4.632
12.540	5.965
11.500	7.245
10.545	8.975
9.670	11.091
8.866	13.857
8.130	17.433
7.455	22.307
6.837	28.667
6.269	37.345
5.749	48.652
5.272	63.652
4.835	82.908
4.433	107.064
4.065	138.238
3.727	176.900
3.418	220.135
3.135	265.330
2.875	307.548
2.636	337.973
2.417	359.502
2.216	360.037
2.033	358.540

$$(176.0 - 33.93), \qquad (31.11 - 28.53), \qquad (26.16 - 22.00)$$

This leads to the set of values $\{d_j, N_j\}$ in Table 3.

Note that over 1000 particles have diameter $d_j \leq 2.417$ (the three smallest classes), whereas the three smallest classes for the 200-μm cut sum to fewer than 450.

The corresponding pack (after roundoff, for 3001 particles) is shown in Fig. 3, and the packing fraction is 0.77788. In other words, the 20-μm cut alone can be the basis for a stoichiometric mix. Figure 4 shows plots of volume fraction, number fraction, and partial volume fraction, and should be compared with the 200-μm data of Fig. 2.

Table 4 shows the true data for a 50-μm cut, and Table 5 shows the values of $\{d_j, N_j\}$ for 3000 particles with a 5-μm cutoff (volume fraction discarded = 0.091, volume fraction kept = 0.909). The following classes have been consolidated:

$$(418.6 - 95.96), \qquad (88.0 - 80.70), \qquad (74.00 - 67.86)$$

The pack, shown in Fig. 5, defines a packing fraction of 0.7887. Figure 6 shows variations in volume fraction, packing fraction, and partial volume fraction.

Here the modified cut differs significantly from the true cut because 9.1% of the volume has been discarded, all of it fine powder. This could conceivably affect the burning rate but not necessarily, because a great deal of fine powder has been retained; over 1000 particles have $d_j \leq 5.749$ and belong to the two smallest classes. One possible strategy for accounting for all of the fine powder starts with the construction of a partial pack from the modified cut. The packing algorithm defines a dynamic process in which the packing fraction starts at 0 and grows with time until it reaches a maximum; partial pack is achieved when this process is cut off prematurely.[2]

Let us suppose that, using the modified cut, we construct a partial pack with packing fraction x. To this we add $(0.091/0.909)x$ of fine powder uniformly dispersed in the binder (homogenized) so

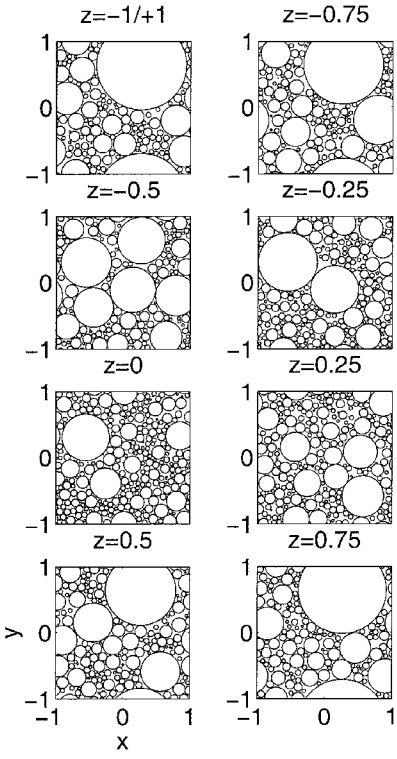

Fig. 3 Slices through a 20-μm pack, packing density 0.77788.

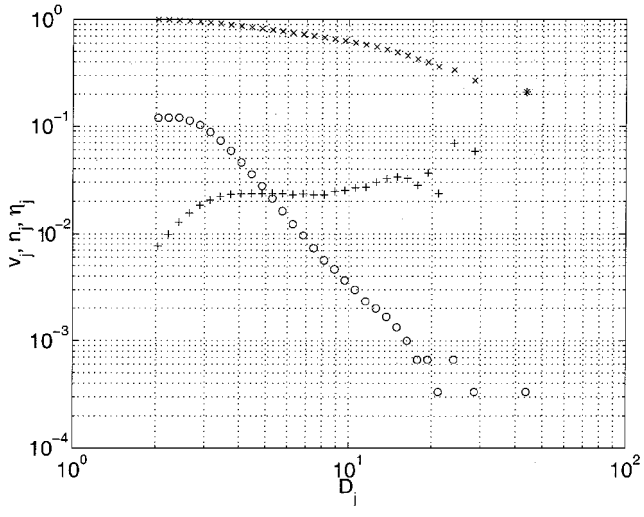

Fig. 4 Volume fraction (+), number fraction (○), and partial volume fraction (×) as a function of particle diameter for the 20-μm data.

that the total volume fraction of AP is $1.1x$. If we require this to be 0.78, it follows that x must be 0.71. The pack is then composed of a fraction 0.71 of discrete AP particles of known size and location and a fraction 0.07 of fine AP blended with a fraction 0.22 of binder as a homogeneous mixture. (Note that there will be a minimum AP size that can be resolved by the combustion code once the largest particles are assigned, and it is quite likely that some of the discrete particles will also have to be homogenized to satisfy this constraint.) We can reasonably expect that there will be room for the fine powder in the interstitial space between the discrete particles because we know that the desired packing fraction can be achieved without use of the powder.

As a final example of the use of this strategy, we consider propellant mixes defined by Miller,[4] starting with what he calls SD-III-88-24, which consists of 31.58% (by weight) of a 200-μm cut, 42.11% of a 50-μm cut, and 13.68% of a 20-μm cut, for a total of 87.4% by weight of AP, equivalent to a volume fraction of 0.766. We do not know the details of the cuts used by Miller, and so we shall use the Thiokol data.

Table 4 Experimental 50-μm AP data

Channel, μm	% Pass	% In channel
418.6	100	0.03
383.9	99.97	0.07
352.0	99.90	0.17
322.8	99.73	0.24
296.0	99.49	0.29
271.4	99.20	0.35
249.9	98.85	0.44
228.2	98.41	0.56
209.3	97.85	0.71
191.9	97.14	0.90
176.0	96.24	1.13
161.4	95.11	1.40
148.0	93.71	1.72
135.7	91.99	2.05
124.5	89.94	2.39
114.1	87.55	2.71
104.7	84.84	3.02
95.96	81.82	3.26
88.00	78.56	3.41
80.70	75.15	3.48
74.00	71.67	3.48
67.86	68.19	3.44
62.23	64.75	3.34
57.06	61.41	3.21
52.33	58.20	3.06
47.98	55.14	2.92
44.00	52.22	2.77
40.35	49.45	2.62
37.00	46.83	2.47
33.93	44.36	2.31
31.11	42.05	2.24
28.53	39.81	2.10
26.16	37.71	2.01
23.99	35.70	1.93
22.00	33.77	1.87
20.17	31.90	1.81
18.50	30.09	1.81
16.96	28.28	1.75
15.56	26.53	1.70
14.27	24.83	1.65
13.08	23.18	1.58
12.00	21.60	1.52
11.00	20.08	1.44
10.09	18.64	1.37
9.250	17.27	1.30
8.482	15.97	1.25
7.778	14.72	1.20
7.133	13.52	1.16
6.541	12.36	1.12
5.998	11.24	1.09
5.500	10.15	1.05
5.044	9.10	1.02
4.625	8.08	0.98
4.241	7.10	0.95
3.889	6.15	0.91
3.566	5.24	0.85
3.270	4.39	0.79
2.999	3.60	0.70
2.750	2.90	0.61
2.522	2.29	0.52
2.312	1.77	0.42
2.121	1.35	0.35
1.945	1.00	0.28
1.783	0.72	0.24
1.635	0.48	0.21
1.499	0.27	0.16
1.375	0.11	0.08
1.261	0.03	0.03
1.156	0.00	0.00

Table 5 Packing data 50-μm AP

d_j	N_j
117.640	1.102
80.513	1.104
67.750	1.861
59.645	1.317
54.695	1.641
50.155	2.029
45.990	2.511
42.175	3.089
38.675	3.789
35.465	4.632
32.520	5.619
29.820	7.066
27.345	8.591
25.075	10.665
22.995	13.278
21.085	16.687
19.335	20.947
17.730	27.166
16.260	34.052
14.915	42.860
13.675	53.972
12.540	67.024
11.500	83.602
10.545	102.729
9.670	126.739
8.866	156.037
8.130	194.584
7.455	242.225
6.837	303.620
6.269	380.179
5.749	479.864
5.272	599.421

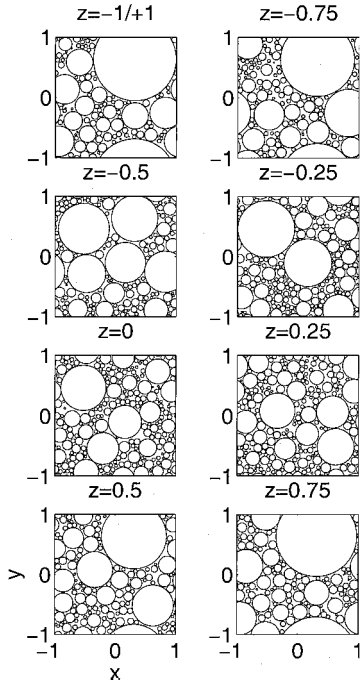

Fig. 5 Slices through a 50-μm pack, packing density 0.7887.

With $N = 10{,}000$, all particles smaller than 5μ are discarded, and then the three modified cuts are mixed according to the fractions specified by Miller.[4] None of the 200-μm cut is discarded, a fraction 0.091 of the 50-μm cut is discarded, and a fraction 0.2168 of the 20-μm cut is discarded. These are equivalent, for the mixture, to discarding a fraction 0.0839. Packing data (rounded off, with $N = 9999$) are shown in Table 6, and a packing realization is shown in Fig. 7, which defines a packing fraction of 0.7698.

We have also constructed 10,000 particle packs of SD-III-88-19 (31.58% of 200 μm, 55.79% of 20 μm) and SD-III-88-23 (42.11% of 200 μm, 31.58% of 50 μm, 13.68% of 20 μm) each having an experimental volume fraction of 0.766. The numerical values are 0.7674 and 0.7900. In each case a significant fraction of small particles is discarded. For example, for SD-III-88-23, 0.091 (volume measure) of the 50-μm cut is discarded, 0.2168 of the 20-μm cut, so that the total volume fraction discarded is 0.0737. If we assume that all of this discard could be homogenized into the binder, the modified pack would have an AP volume fraction of 0.85 rather than 0.79.

Table 6 Data (rounded) for blend corresponding to SD-III-88-24 of Miller[4]

d_j	N_j
211.004	1
126.505	1
88.991	1
87.751	2
77.350	1
75.023	1
70.930	2
65.045	2
59.645	3
54.695	3
52.062	1
50.155	4
45.990	6
42.175	8
38.675	10
35.465	12
32.520	16
29.820	20
27.345	25
25.075	32
22.995	41
21.085	52
19.335	66
17.730	86
16.260	109
14.915	138
13.675	172
12.540	217
11.500	268
10.545	330
9.670	408
8.866	505
8.130	632
7.455	796
6.837	1008
6.269	1284
5.749	1642
5.272	2094

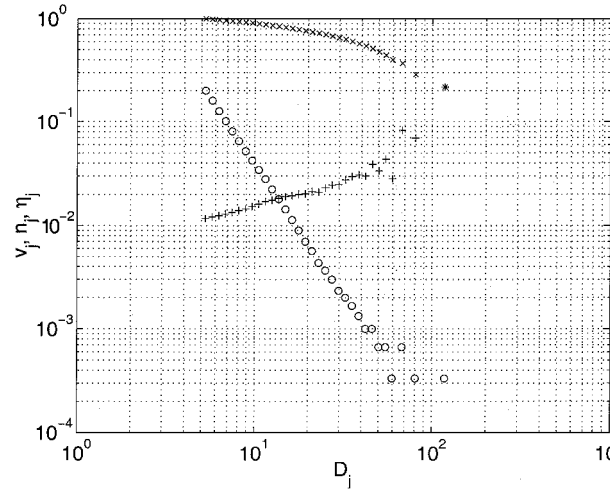

Fig. 6 Volume fraction (+), number fraction (○), and partial volume fraction (×) as a function of particle diameter for the 50-μm data.

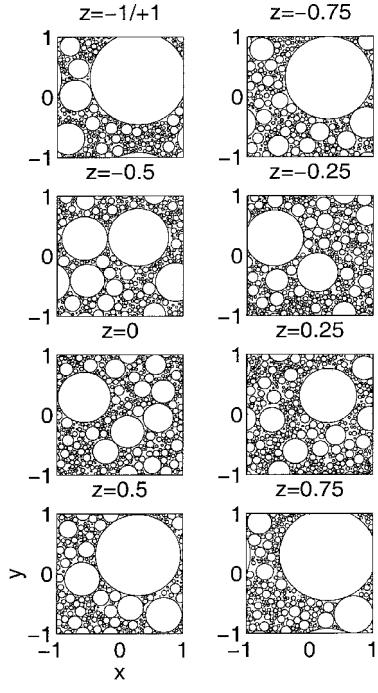

Fig. 7 Slices through a Miller[4] SD-III-88-24 pack, packing density 0.7698.

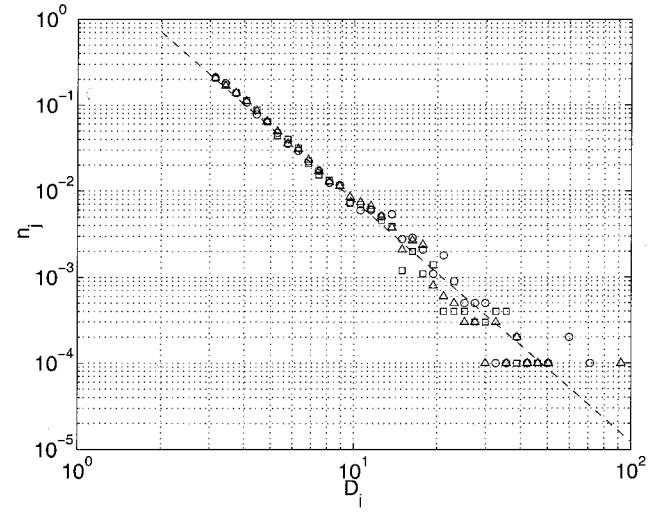

Fig. 8 Number fraction as a function of particle diameter for the 20-μm data, random selection strategy: ○, randseed = 0; □, randseed = 1; △, randseed = 3; and − − −, least-squares fit.

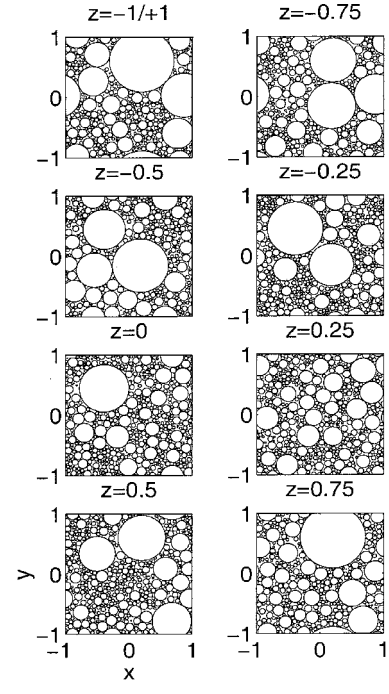

Fig. 9 Slices through the 20-μm pack defined by the random selection method, randseed = 0.

III. Random Selection Strategy

In this section we describe an alternative strategy for defining a pack using the experimental data. The packing algorithm is random in nature, in the sense that the inital locations of the particle centers are randomly assigned. What is shown in Figs. 1, 3, 5, and 7 are single realizations, and different initial data would generate different realizations. (Provided N is sufficiently large, as here, the variations in packing fraction between one realization and another are small.) A random strategy can also be used to convert the experimental data into packing data.

Consider the set $\{d_j, n_j\}$ for one of the cuts, for example, (fourth and fifth columns of Table 1). If the $\{n_j\}$ are multiplied by a sufficiently large number, they can all be converted to integer values, and in principle, we could use these values to define a pack. In practice, however, the number of particles so defined, M, is too large to handle computationally. However, we can reduce the number by random sampling. A counting integer is assigned to each particle so that particles $(1, 2, \ldots, i_1 - 1)$ have diameter d_1, particles $(i_1, i_1 + 1, \ldots, i_2 - 1)$ have diameter d_2, etc., and in this way the total of M particles are numbered. A single integer is then randomly chosen from the set of integers, thus selecting a particle, and this is repeated N times, where N is the number of particles to be used in the pack. If this entire process were repeated a large number of times, the number fraction for each diameter averaged over all realizations would be that for the entire set of particles. Provided N is sufficiently large, each realization will be representative of the true pack. Moreover, variations between each realization, a cube of propellant, will correspond to variations between random cubes cut from the true pack.

In the earlier strategy, averaging is carried out (via consolidation) before the packing data is defined, and the stochastic ingredients are introduced only when packs are created from that data. In the present strategy a stochastic ingredient is introduced in the selection of the data.

We present results for the 20-μm experimental data shown in Table 2, but discard particles smaller than 3 μm (with volume fraction 0.0857). We take 10,000 particles, randomly chosen by the strategy described earlier. The random sequence is defined by using a random number generator parameter (randseed). Calculations are carried out for four different random sequences, and Fig. 8 shows number fraction/particle diameter scatter plots for three of these. There are differences for the larger diameters and, in general, as other calculations that we have carried out, not reported here, make clear, the smaller the number of particles in the pack, the smaller the diameters for which these differences are first apparent. A least-squares fit to these data is

$$\log(n_j) = 1.6194 - 2.8041 \log(D_j)$$

(natural logarithms), which suggests an obvious strategy for defining a single representative pack.

The target packing density is 0.77, and the code is stopped if this value is reached. Then the achieved packing fractions corresponding to randseed = 0, 1, 2 are 0.7702, 0.7464, 0.7426. The fourth seed yields a packing fraction of 0.7702. The differences in these results appear to be linked to the different distributions of large particles. The first pack has one 71-μm particle, two 60-μm particles, one 50-μm particle, etc.; the fourth pack has one 92-μm particle, one 50-μm particle, etc. On the other hand, the second and third packs each have one 46-μm particle, and no larger ones. This serves to reinforce the obvious fact that the manner in which the large particles should be represented is a delicate one when there are few large particles in the pack, and a certain resolution can only be achieved if large (100,000 or more particles) packs are considered.

Slices through packs 1 and 2 (randseed = 0, 1) are shown in Figs. 9 and 10.

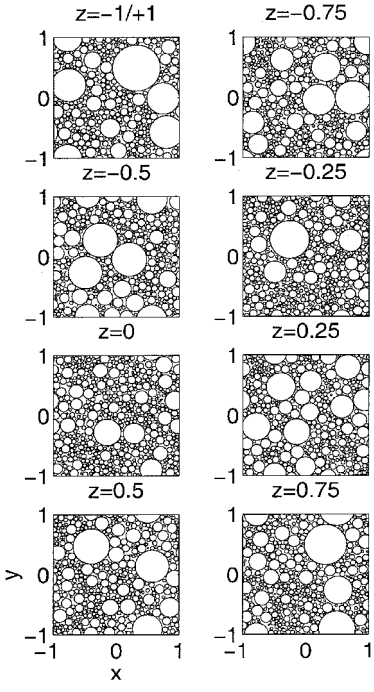

Fig. 10 Slices through the 20-μm pack defined by the random selection method, randseed = 1.

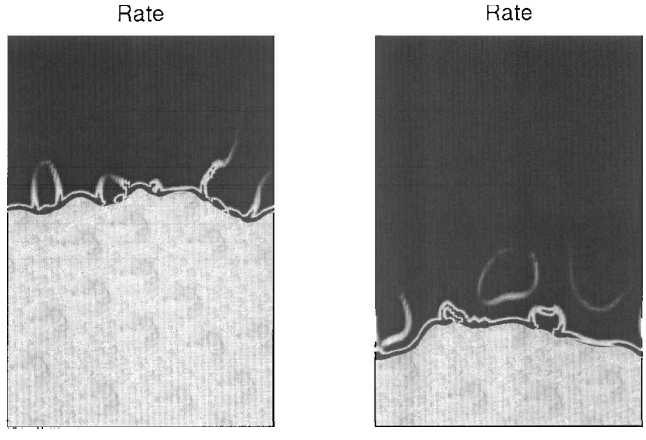

Fig. 11 Reaction-rate contours at two times.

IV. Combustion Field

Packing algorithms have a number of applications, but our concern is to generate physically meaningful data that can be used in propellant flame calculations. It is not our purpose to discuss in detail such calculations, but rather to put some purpose to the abstract structures discussed here. To this end we have performed preliminary flame calculations for a two-dimensional propellant, one where the AP particles are represented by disks rather than spheres. We consider a binary pack (diameters 189.8 and 47.45 μm) and the nature of the pack is partly apparent from Figs. 11 and 12. The packing fraction is 0.803, despite the lack of fine powder, a consequence of the two-dimensional nature: A circle inscribed in a square occupies a fraction $\pi/4$ of the square, whereas a sphere inscribed in a cube occupies but a fraction $\pi/6$ of the cube.

To describe the physics within the solid (condensed phase) it is convenient to use a level-set function $\psi(x, y)$ so that a point (x, y) lies in the AP if $\psi \geq 0$ and in the binder if $\psi < 0$. Then we solve the heat equation

$$\rho_c \frac{\partial T}{\partial t} = \frac{\lambda_c}{C_p} \nabla^2 T \tag{7}$$

where ρ_c and λ_c are assigned appropriate values according to the sign of ψ. For convenience, the value of the specific heat is set equal to C_p (constant) for the gas.

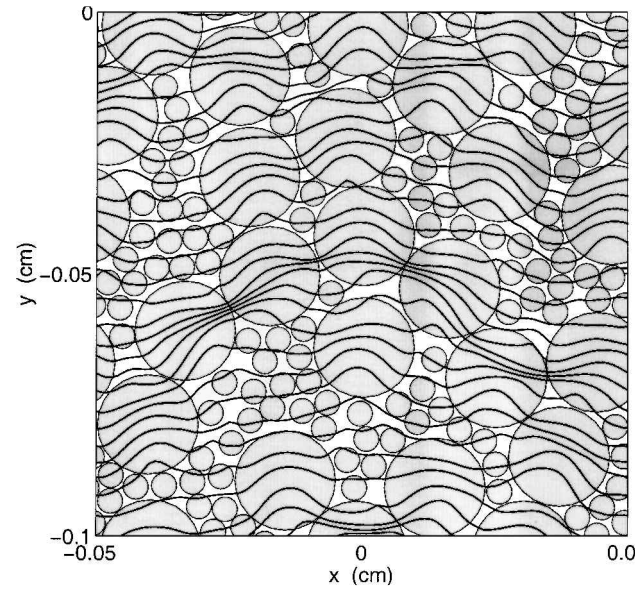

Fig. 12 Surface positions at equal time intervals.

In the gas we account for two reactions,

$$X \xrightarrow{R_1} Z, \qquad \beta Z + Y \xrightarrow{R_2} \text{final products}$$

with the first corresponding to AP decomposition and the second to reaction between the decomposition products and the binder. Here β defines the overall stoichiometry, the mass of AP that combines stoichiometrically with a unit mass of binder. If we assume that the pack is stoichiometric and that the AP density is 1.95 g/cm^3 and the binder density 0.92 g/cm^3, then $\beta = 8.64$.

The governing equations in the gas are, in principle, the familiar ones; it need only be noted that temperature-dependent transport is accounted for, but the three Lewis numbers are set equal to 1. We write "in principle," however, because an Oseen approximation reduces the computational burden and yet has been proven accurate in calculations that we have done for periodic sandwich propellants.[3] In this approximation, the momentum equation is discarded, and the flow is replaced by a parallel shear flow in the y direction (y is measured perpendicular to the flat unburnt propellant surface). The magnitude of this flow (x dependent) is consistent with mass conservation at the propellant surface. As the shape of the surface and the local regression rate fluctuate, the magnitude of the flow fluctuates, fluctuations that are felt instantaneously for all y. This is consistent with the assumption that the gas phase is quasi steady because as the timescale is controlled by the physics within the solid.

The third numerical ingredient is concerned with the surface regression. We assume that the surface can be characterized by a single-valued function $\phi(x, t)$, namely,

$$\eta \equiv y - \phi(x, t) = 0 \tag{8}$$

Then the function η satisfies the equation

$$\frac{\partial \eta}{\partial t} - r_b |\nabla \eta| = 0 \tag{9}$$

where r_b is the local regression rate (the speed with which the surface moves in the normal direction), defined by simply pyrolysis laws, namely,

$$r_b = \begin{cases} r_{AP} = A_{AP} \exp\{-E_{AP}/R_u T_{AP,s}\} & \psi \geq 0 \\ r_B = A_B \exp\{-E_B/R_u T_{B,s}\} & \psi < 0 \end{cases} \tag{10}$$

Equations (7) and (9) are solved simultaneously with the gas-phase equations, with appropriate connection conditions at the surface. These conditions allow for exothermic/endothermic processes,

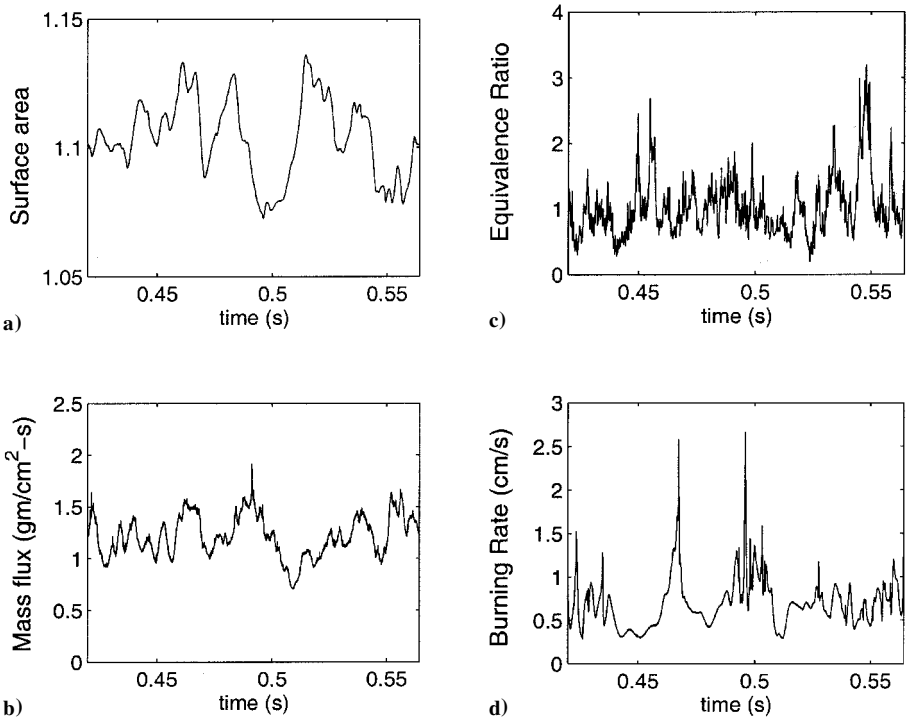

Fig. 13 Surface properties of the burning propellant.

as conventionally discussed. The variable $\eta(x, y, t)$ is used in place of y in the field equations in both the solid and the gas, fixing the surface at $\eta = 0$.

Plausible choices are made for the various parameter values (see Ref. 3), and we shall confine our remarks here to the gas-phase kinetic parameters. The reaction rates are assumed to have the form

$$R_1 = D_1 P^{n1} X \exp\{-E_1/R_u T\}$$

$$R_2 = D_2 P^{n2} ZY \exp\{-E_2/R_u T\} \tag{11}$$

The six parameters here are chosen to satisfy experimental data (regression rate and temperature sensitivity) for pure AP burning,[5] and the burning of an infinitesimally fine blend of AP in binder,[6] both one-dimensional combustion fields. Details are given in Ref. 7 and yield the results

$$E_1/R_u = 8000\ \text{K}, \qquad E_2/R_u = 11000\ \text{K}$$

$$D_1 = 1.3718 \times 10^4\ \text{g/cm}^{-3} \cdot \text{s}^{-1}\ \text{bar}^{-n_1}, \qquad n_1 = 1.7$$

$$D_2 = 3.6768 \times 10^4\ \text{g/cm}^{-3} \cdot \text{s}^{-1}\ \text{bar}^{-n_2}, \qquad n_2 = 1.8$$

At 20 atm, pure AP burns at ~0.28 cm/s, and a fine AP/binder blend burns at ~1.1 cm/s. The average burning rate for the pack is ~0.69 cm/s, an intermediate value. Figure 11 shows reaction rate contours at two different times, as the pack burns through, and gives some indication of the complexity of the combustion field. Figure 12 shows the surface location at equally spaced time intervals; there is a clear tendency for the surface to move more rapidly through regions where the small AP particles are clustered than through the large AP particles. Figure 13 shows variations in various surface quantities as a square of propellent is consumed (overall the propellant is represented by a periodic array of randomly packed squares, and the total time interval shown here is essentially one period).

Figure 13a shows variations in the surface area, roughly 10% greater than that of a flat surface. Figure 13b shows variations in the integrated normal mass flux through the surface. The average density of the pack is 1.747 g/cm^3 so that an average regression rate of 0.69 cm/s corresponds to an average mass flux of 1.205 g/cm^3· s. Figure 13d shows variations in the maximum burning rate, and there are notable excursions above that mean. These excursions vary over time intervals of just a few milliseconds.

Perhaps of greatest interest is Fig. 13c. This shows the surface integrated flux of fuel divided by the surface integrated flux of AP, normalized by the stoichiometric proportion of these fluxes. It can be called the integrated flux-based equivalence ratio. Excursions above 2 and below $\frac{1}{2}$ occur, so that at times the gases being swept away from the surface are strongly fuel rich on average, at other times strongly fuel lean.

V. Concluding Remarks

In this paper we have examined how spheres of various sizes can be packed to generate models of propellant morphology that can be used in combustion calculations. We have examined the problem in some detail and used a significant amount of industrial data to demonstrate that realistic packing fractions can be achieved because we believe that the strategy will become a standard for the study of propellant burning.

To give some insights into the kinds of questions that can be examined once a model propellant has been constructed, we present some preliminary results for the burning of a two-dimensional propellant. Three-dimensional calculations are possible in a parallel computing environment, and we expect to report on such calculations in the future. We also expect to explore a variety of fundamental questions long discussed by the propellant community using intuitive arguments and/or one-dimensional models. These include the effects of pressure and time-dependent pressure fluctuations on the burning rate, the effects of velocity disturbances originating in the chamber flow, the effects of AP size and size distribution, and the effects of stoichiometry. In addition we expect to explore the manner in which the strong surface fluctuations that we have identified in Fig. 13 could effect the nature of the turbulent field within the chamber and how such fluctuations might interact with acoustic waves within the chamber. At the same time, we expect to increase the complexity of the model, including, for example, aluminum combustion and radiation effects.

Acknowledgments

This work was supported by the U.S. Department of Energy through the University of California under Subcontract B341494.

J. Buckmaster is also supported by the Air Force Office of Scientific Research. The authors are indebted to R. Bennett of Thiokol Corporation for suppling the experimental packing data used in this paper.

References

[1]Jackson, T. L., Buckmaster, J., and Hoeflinger, J., "Three-Dimensional Flames Supported by Heterogeneous Propellants," *Proceedings of the Combustion Institute*, Vol. 28, 2000, pp. 895–902.

[2]Knott, G. M., Jackson, T. L., and Buckmaster, J., "The Random Packing of Heterogeneous Propellants," *AIAA Journal*, Vol. 39, No. 4, pp. 678–686.

[3]Hegab, A., Jackson, T. L., Buckmaster, J., and Stewart, D. S., "Nonsteady Burning of Periodic sandwich Propellants with Complete Coupling Between the Solid and Gas Phases," *Combustion and Flame*, Vol. 125, Nos. 1/2, pp. 1055–1070.

[4]Miller, R. R., "Effects of Particle Size on Reduced Smoke Propellant Ballistics," AIAA Paper 82-1096, June 1982.

[5]Beckstead, M. W., Tanaka, M., Jing, Q., and Jeppson, M. B., "An Ammonium Perchlorate Model Based on a Detailed Mechanism," *33rd JANNAF Combustion Meeting*, CPIA Publ. 638, Chemical Propulsion Information Agency, Laurel, MD, 1996, pp. 41–46.

[6]Jeppson, M. B., Beckstead, M. W., and Jing, Q., "A Kinetic Model for the Premixed Combustion of a Fine AP/HTPB Composite Propellant," *35th JANNAF Combustion Meeting*, CPIA Publ. 680, Chemical Propulsion Information Agency, Laurel, MD, 1998, pp. 639–654.

[7]Buckmaster, J., Jackson, T. L., Hegab, A., and Kochevets, S., "Modeling Propellants and Modeling Propellant Flames," 37th JANNAF Combustion Meeting, 2000.